Quantifying variability of incipient-motion thresholds in gravel-bedded rivers using a grain-scale force-balance model

Scott A. Feehan[1], Scott W. McCoy[1], Joel S. Scheingross[1], and Michael H. Gardner[2]

[1]Department of Geological Sciences and Engineering, University of Nevada, Reno, NV, USA
[2]Department of Civil and Environmental Engineering, University of California, Davis, CA, USA

Key Points:

- Using a grain force-balance model and observed parameter distributions, we quantify expected variability in incipient-motion thresholds
- Predicted distributions of incipient-motion thresholds match those observed in laboratory experiments and natural rivers
- A power law can describe mean threshold of motion and its variability for the relationship between grain size and threshold velocity

Corresponding author: Scott A. Feehan, `sfeehan@nevada.unr.edu`

Abstract

Predicting thresholds of sediment motion is critical for a range of applications involving sediment transport. However, thresholds for sediment motion can vary over an order of magnitude for a single characteristic flow and bed configuration. Lacking simple ways to incorporate this variability, many assume thresholds are constant for rough, turbulent flow. Here, we quantify variability of incipient-motion thresholds based on a commonly used grain-scale force-balance model, with model parameter distributions determined from published experiments. We show that variability in the threshold of motion within the 2D force-balance model occurs predominantly due to variability in the lift coefficient and grain protrusion, and secondarily due to drag coefficient variability. For a known grain size, the mean threshold of motion, and variability about the mean, can be predicted from a family of power laws. These power laws can be altered with site-specific parameter distributions, allowing for site-specific application to well-studied reaches and other planets. Using compiled flume and field data we show that constraining force-balance parameter distributions with independent data results in narrower distributions of the predicted threshold of motion, consistent with constrained flume experiments. This analysis highlights that while the threshold of sediment motion is variable, the magnitude of variability is predictable within the force-balance model based on site-specific physical constraints of local flow and bed conditions.

Plain Language Summary

Understanding what flow velocities are needed for rivers to move gravel and boulders is critical for river management, reducing flood hazards, understanding river ecosystems, and the long-term evolution of landforms such as deltas and mountain ranges. However, accurate predictions of sediment transport are made challenging by large variability in flow conditions observed when a particular size of sediment is moved by a river. In this work we use an existing theory to explore the expected flow conditions and flow variability needed to move sediment. These results allow for more accurate river restoration and engineering designs and more sustainable river management.

1 Introduction

When predicting sediment transport using popular empirical, deterministic approaches, a threshold of motion is required to define the condition below which sediment is static and above which sediment transport occurs (e.g., τ_c^*=0.045, where τ_c^* is the critical Shields stress for grain motion (Shields, 1936; Buffington & Montgomery, 1997)). This approach has been used in a variety of applications, including predicting the magnitude of bedload flux (e.g., Meyer-Peter & Müller, 1948; Fernandez Luque & Van Beek, 1976; Yager et al., 2007), understanding the hydraulic geometry of river channels (e.g., Parker, 1978; Pfeiffer et al., 2017; Phillips et al., 2022), modeling deposition, erosion, and subsequent evolution of river profiles (e.g., Parker, 1991; Wickert & Schildgen, 2019), predicting the occurrence of suitable habitat for aquatic organisms (e.g., Riebe et al., 2014; Wohl et al., 2015) and estimating the magnitude of past floods on Earth, Mars and other planetary bodies (e.g., Baker, 2002; Perron et al., 2006; Williams et al., 2013).

Many methods exist to estimate the threshold of motion. For example, the threshold can be quantified as a critical value of a non-dimensional parameter, such as τ_c^*, which roughly scales with the ratio of fluid stress on the grain to the grain weight, or as dimensional parameters such as the critical shear stress on the grain τ_c or a critical velocity near the grain u_c when motion first begins (Wiberg & Smith, 1987; Buffington & Montgomery, 1997; Garcia, 2008). Theory to predict these thresholds often use a force-balance approach (e.g., Wiberg & Smith, 1987). In this case, motion is predicted to occur when the forces promoting grain motion (e.g., fluid drag and lift) exceed the forces resisting motion (e.g., the grain weight and friction). The force-balance method can predict threshold conditions for τ_c^*, τ_c, and u_c, and can be estimated using common field measurements (e.g., grain-size distribution and channel slope) combined with generalized assumptions about fluid drag. The ease of application of the force-balance method has led it to be perhaps the most commonly applied mechanistic method to predict the threshold of motion (e.g., Kirchner et al., 1990; Bridge & Bennett, 1992; Vollmer & Kleinhans, 2007; Recking, 2009; Scheingross et al., 2013; Prancevic et al., 2014; Lamb et al., 2017a; Yager, Schmeeckle, & Badoux, 2018).

However, not every underlying process that controls the onset of motion is captured in the force-balance framework. Recent work has demonstrated the importance of turbulent burst durations (known as impulse) (e.g., Diplas et al., 2008; Celik et al., 2013), moment and torque balances (e.g., Smart & Habersack, 2007; Lee & Balachandar, 2012; Dey & Ali, 2018), and the mechanism of grain entrainment (e.g., establishing different criterion for initial particle motion via rolling, sliding or lifting of a grain out of its pocket) (Pähtz et al., 2020). These recently developed approaches require more complex measurements to properly estimate the threshold of motion, such as estimating local inertial forces (e.g., Maniatis et al., 2020), high resolution flow turbulence data and/or a priori knowledge of the dominant entrainment mechanism (e.g., Dey & Ali, 2017a). These requirements make these newly developed approaches more difficult to apply than the simple force balance, and hence the simple force balance, despite its shortcomings, remains in use. Furthermore, the force-balance approach is used and performs well in lab experiments, even when underlying model assumptions such as spherical grains, are broken (e.g., Prancevic & Lamb, 2015; Deal et al., 2023), and can explain a wide breadth of field and flume data (e.g., Lamb et al., 2008), where additional model assumption break down.

All of the above-mentioned methods to estimate the threshold of motion are deterministic; given known input parameters, the models output a single value for the threshold of motion. Field and flume data show there is not a single value for the onset of sediment motion, and instead, there is variability around a mean estimate. For example, in gravel-bedded rivers with slopes less than 5%, the critical Shields number is often estimated as $\tau_c^* \approx 0.045$, but experimental and field observations show that τ_c^* values can range from approximately 0.02 to 0.09 (Buffington & Montgomery, 1997). This variability may arise due to local differences in particle shape, flow characteristics, grain packing, style of initial motion (e.g., rolling vs sliding) and more (e.g., Kirchner et al., 1990; Hodge et al., 2013; Yager, Schmeeckle, & Badoux, 2018; Deal et al., 2023); but limited work to date (e.g. Lee & Balachandar, 2012) has shown how variations in these physical characteristics propagate through the force-balance model to set variability in observed incipient motion.

Here, we focus on estimating expected variability of the threshold of motion using the Wiberg and Smith (1987) force-balance model. While our analysis can be performed on other models (e.g., Dey & Ali, 2018; Pähtz et al., 2020), we explore the force-balance model because of its ease of application and common use. Furthermore, because the input parameters to the force-balance model are the most well constrained of any initial-motion model, using the force-balance model allows us to best explore how variability in model input parameters results in variability in the threshold of motion. In this sense, our goal is solely to describe expected variability within an existing model framework. While our work may yield insights on properties that control incipient motion within the force-balance model, we do not seek to fundamentally advance upon existing mechanistic descriptions of incipient motion.

Predicting the threshold of motion with the force-balance model requires several input parameters, which we refer to as force-balance parameters (FBPs). Variability in turbulent fluid stresses, bed packing, grain exposure, and grain geometry result in FBP variability, and ultimately affect the threshold of motion (e.g., Shields, 1936; Grass, 1970; Gessler, 1971; Paintal, 1971; Kirchner et al., 1990; Church et al., 1998; Schmeeckle et al., 2007; Diplas et al., 2008; Booth et al., 2014; Lamb et al., 2017a; Yager, Schmeeckle, & Badoux, 2018; Masteller et al., 2019; Hassan et al., 2020). We hypothesize that a majority of the scatter in the threshold of motion observed in gravel-bed rivers is predictable and can be explained by expected FBP variability. Here, we quantify variability in the threshold of motion explicitly with expected distributions of critical velocity and critical shear stress at the onset of sediment motion. We do this by first quantifying the expected variability in each FBP using published laboratory experiments and detailed field studies, we then use a Monte Carlo method to propagate FBP variability through a deterministic force balance to estimate critical velocity and shear stress distributions at incipient motion. Constraining this variability allows us to quantify the expected variability in the threshold of motion, ultimately providing more robust, even if uncertain, sediment transport estimates.

2 Force-balance framework

2.1 Theoretical framework

Particle motion occurs when the forces promoting motion exceed the forces resisting motion (e.g., Wiberg & Smith, 1987). The forces promoting particle motion include the lift force, F_L, drag force, F_D, and the downslope component of the buoyant weight, calculated as $(F_G - F_B)\sin(\beta)$, where F_B is the buoyant force, F_G is the gravitational force and β is the bed angle). We assume the buoyant force operates in the direction opposing the gravity vector and is vertical in our coordinate system (Wiberg & Smith, 1987; Chiew & Parker, 1995) rather than normal to the water surface as in Christensen (1995). The forces resisting motion, F_R, are the bed-normal component of the buoyant weight, F_N, and friction. The threshold of motion occurs when the forces promoting and resisting motion are balanced

$$F_D + (F_G - F_B)\sin(\beta) = F_R. \tag{1}$$

Following Wiberg and Smith (1987), we define the forces acting on the grain as

$$F_D = \frac{1}{2} C_D \rho A_e u^2 \tag{2}$$

$$F_L = \frac{1}{2} C_L \rho A_p u^2 \tag{3}$$

$$F_B = \rho g V_P \tag{4}$$

$$F_G = \rho_s g V_P \tag{5}$$

$$F_R = F_N \tan(\phi) = [(F_G - F_B)\cos(\beta) - F_L]\tan(\phi) \tag{6}$$

where g is gravitational acceleration, and ϕ is the effective friction angle that parameterizes geometric and frictional resistance and is commonly written as the effective coefficient of friction $\mu = \tan(\phi)$. C_D and C_L are the effective drag and lift coefficients, respectively, ρ and ρ_s are the fluid and sediment densities, respectively and u is the downstream flow velocity proximal to the grain (Schmeeckle et al., 2007). A_e is the upstream-facing cross-sectional area of the grain exposed to the flow. We calculate A_e assuming spherical grains as $A_e = A_n - A_b$, where $A_n = \pi r^2$ is the full upstream-facing cross-sectional area of the grain in the plane perpendicular to the mean bed surface, with r as the radius of the grain and A_b is the cross-sectional area of the grain that is buried or obscured from the flow, calculated as

$$A_b = r^2 cos^{-1}((r-(D-p))/r) - (r-(D-p))\sqrt{2r(D-p)-(D-p)^2} \tag{7}$$

where p is the grain protrusion (defined as the height of the grain above the local mean bed elevation). A_p is the cross-sectional area of the grain in the plane parallel to the mean bed surface and is the area over which F_L is assumed to act. A_p is equivalent to the full cross-sectional area of the grain, A, when the relative protrusion value ($p_* = p/D$) is ≥ 0.5. When $p_* < 0.5$, we calculate A_p as

$$A_p = \pi(r^2 - (r-p)^2) \tag{8}$$

(Figure 1a). These geometric definitions of A_e and A_p are dependent on the assumption of spherical grains with particle volume $V_p = 4/3\pi(D/2)^3$. We use the term 'effective' to describe parameters that depend on multiple factors, either owing to our use of simplified equations that neglect variably important physics, as in the case of F_D and F_L (Schmeeckle et al., 2007; Diplas et al., 2008; Celik et al., 2013; Dey et al., 2020), or are inherently formulated to include multiple contributing effects that are scale dependent, as in the case of ϕ (Booth et al., 2014; Yager, Schmeeckle, & Badoux, 2018). Similarly, because observations of ϕ and C_D are based on lab and field studies using natural grains mobilized via a mix of rolling and sliding, variability in observed distributions should capture the expected variability from the presence of non-spherical grains and different modes of initial motion. We use a 2D force balance to maintain consistency with previous work and we assume that the flow conditions at the time of entrainment are fully turbulent (Komar & Clemens, 1986; Lamb et al., 2008; Scheingross et al., 2013; Prancevic & Lamb, 2015; Ali & Dey, 2018). To avoid the complications of steep slopes and/or shallow flows on sediment mobilization, we further assume that the bed slope is constant at $\tan(\beta) = 10^{-3}$ and that grains are fully submerged within the flow.

We frame the threshold forces acting on the grain in terms of a critical grain-proximal velocity, u_c, by first substituting Equations (2) - (6) into Equation 1 to obtain an equality defining the critical state at initiation of motion

$$\frac{1}{2}C_D \rho A_e u_c^2 + (\rho_s g V_P - \rho g V_P)\sin(\beta) = ((\rho_s g V_P - \rho g V_P)\cos(\beta) - \frac{1}{2}C_L \rho A_p u_c^2)\tan(\phi) \tag{9}$$

and we rearrange Equation 9 to isolate u_c

$$u_c = \left(\frac{2(\rho_s/\rho - 1)gV_P\,(\cos(\beta)\tan(\phi) - \sin(\beta))}{C_D A_e + C_L A_p \tan(\phi)}\right)^{0.5}. \tag{10}$$

Equation 10 defines the grain-proximal downstream flow velocity that must be exceeded to initiate sediment motion and is dependent on ρ, ρ_s, C_D, C_L, μ, and p (via A_e and A_p). Equation 10 does not explicitly account for turbulence; however, turbulence influences the value of C_D and C_L, allowing us to account for turbulence through including the large range of C_D and C_L values. The formulation of Equation 10, although often considered to represent a sliding entrainment mechanism, can be used to represent flow conditions necessary for entrainment through other modes by altering the effective friction coefficient to approximate the frictional resistance appropriate for any given mode. For a rolling mode specifically, the effective friction coefficient is lower than that for a sliding mode (Kirchner et al., 1990). We use Equation 10 to explore the influence of variability in the forces governing grain motion. We focus on the grain-scale critical velocity threshold, rather than reach-scale or time-averaged properties (e.g., reach-averaged shear stress or depth-averaged flow velocity), because near-bed fluctuations of flow velocity more accurately describe incipient motion than averaged flow measurements (Kirchner et al., 1990; Schmeeckle et al., 2007; Yager, Schmeeckle, & Badoux, 2018; Yager, Venditti, et al., 2018). Furthermore, using grain-scale velocity permits flow velocity estimates without requiring flow depth estimates. To aid comparison to existing data, we also cast the incipient motion threshold in terms of critical shear velocity, u_{*c}, critical shear stress and critical Shields stress in subsequent sections.

2.2 Variability of force-balance parameters

Estimating the variability in incipient motion using the force-balance framework described above requires quantifying the variability in the FBPs setting the threshold of motion. In this section we use published laboratory experiments and field surveys to develop the most general and broad FBP distributions that could be applicable in natural rivers of low slope (slopes $< 5\%$) with no additional information (e.g., no information on particle size or shape, water discharge, etc.). The distributions of force-balance parameters represent observed variability in space and time measured from independent experiments and field sites. As we show below, measured parameter variability is generally large relative to expected measurement uncertainty such that we assume distributions are dominated by observable variability, not measurement uncertainty. Furthermore, we assume that these limited observations have quantified the expected FBP variability. Many FBPs have documented parameter ranges, but lack quantified distribution forms. In these cases we assume parameters follow truncated normal distributions that have zero probability outside of specified ranges. These FBP distributions can be narrowed with additional site-specific or experiment-specific data (e.g., grain packing and particle density) as demonstrated in later sections.

Force-Balance Parameters						
Parameter Input	Drag C_D	Lift C_L	Friction μ (ϕ)	Relative Protrusion p_*	Fluid density ρ (kg/m^3)	Sediment density ρ_s (kg/m^3)
Mean	0.76	0.65	2.75 (70°)	0.7	1000	2650
Standard Deviation	0.29	0.29	0.27 (15°)	0.4	30	100
Minimum	0.1	0.06	0.27 (15°)	0.1	990	2500
Maximum	3	2	11.4 (85°)	1	1200	3000

Table 1. Values used to create generally applicable force-balance parameter distributions.

Grain and bed properties control the effective frictional resistance to motion (Yager, Schmeeckle, & Badoux, 2018). For a single grain in an idealized pocket geometry, the effective friction coefficient, $\mu = \tan(\phi)$, can be represented as the rotation angle between the grain being mobilized and the contact point with the downstream grain over which mobilization occurs (Figure 1a) (e.g., Wiberg & Smith, 1987). Natural bed sediments, however, are generally confined to pockets in which there are multiple points of contact and the grain may exit oblique to the downstream direction, creating a distribution of μ values that can range from an effective angle (ϕ) of 10 to 90 degrees (Kirchner et al., 1990; Hodge et al., 2013). Furthermore, μ is scale dependent such that the value for single-grain entrainment differs relative to sediment mobilization in force-chain clusters (Booth et al., 2014). Field, flume, and numerical studies commonly document log-normal μ distributions (Kirchner et al., 1990; Booth et al., 2014), with values likely resulting from variable importance of pocket geometry, grain shape and bed packing (Buffington & Montgomery, 1997; Johnston et al., 1998; Hodge et al., 2013; Prancevic & Lamb, 2015; Yager, Schmeeckle, & Badoux, 2018; Deal et al., 2023). We assume μ is log normally distributed around a mean effective friction angle of 70 degrees, a standard deviation of 15 degrees, and is truncated with a minimum and maximum of 15 degrees and 85 degrees, respectively (Table 1), which is representative of many naturally packed sediment beds (Hodge et al., 2013; Prancevic & Lamb, 2015).

The amount of grain protrusion p, adds additional variability as it modulates the grain area normal (A_e) and parallel (A_p) to the bed where F_D and F_L act, respectively (Kirchner et al., 1990; Yager, Schmeeckle, & Badoux, 2018). We use field observations to set the distribution of $p_* = p/D$; we assume p_* is normally distributed with a mean value of 0.7 (i.e., 70% of the grain height is exposed to the flow), and a standard deviation of 0.4 (Yager, Schmeeckle, & Badoux, 2018). We set the minimum p_* value to 0.1 based on field observations from Yager, Schmeeckle, and Badoux (2018) showing that >98% of non-buried grains have $p_* \geq$ to 0.1.

Fluid-grain interactions (as quantified in Equations 2 and 3) depend on effective drag and lift coefficients, C_D and C_L. C_D is commonly assumed to be dependent on grain size, grain shape, and particle Reynolds number, and is assumed to approach a value of 0.4 to 1 for natural channels (Ferguson & Church, 2004). However, near bed velocity fluctuations produce complex flow structures and changing points of flow separation under variable duration of the imposed fluid force, resulting in instantaneous C_D values deviating from the 0.4 - 1 range, even for constant grain size, shape and particle Reynolds number (e.g., Schmeeckle et al., 2007; Celik et al., 2013; Hurst et al., 2021). This variability in C_D is due to variably important physics, including form drag, skin friction and the effects of bed roughness, which are lumped into C_D within the simplified form of equation 2 (Lee & Balachandar, 2017; Dey & Ali, 2017a, 2017b; Li et al., 2019). Similarly, C_L, as represented in Equation 3, encompasses a wide array of processes including shear lift, Magnus lift, centrifugal lift, and turbulent lift that have uncertain relative influence on C_L (Ali & Dey, 2016; Dey et al., 2020). We assume both C_D and C_L follow a truncated normal distribution, with a mean C_D of 0.76 and range of 0.1 - 3, as measured for a spherical particle on a gravel bed in turbulent flow (Schmeeckle et al., 2007). Mean $C_L = 0.85C_D$ (Ali & Dey, 2016) and range from 0.06 - 2. We assume a standard deviation of 0.29 for both C_D and C_L (Einstein & El-Samni, 1949; James, 1990; Schmeeckle et al., 2007; Lamb et al., 2017a; Dey et al., 2020).

The remaining FBPs represent physical properties that, for a particular reach of interest, commonly have a narrow range. For generality, we assume the density of water varies from 0.99 g/cm^3 to 1.2 g/cm^3 (owing to variability in temperature or suspended sediment concentration) and that the density of grains varies with sediment lithology, from 2.5 g/cm^3 for siliciclastic to 3.0 g/cm^3 for mafic grains.

2.3 Potential covariability of force-balance parameters

All FBP distributions presented above are based on empirical observations. In this section, we account for the possibility that FBP values and distributions may covary. The most well established covariability between FBPs is for F_L and F_D, where some represent F_L as the bed normal component of F_D at low slopes (Schmeeckle et al., 2007), while others have argued F_L is independent of F_D across a range of flow conditions (Celik et al., 2013). We assume that C_L and C_D are co-variable such that when sampling from FBP distributions (see Section 4), the same percentile value is selected from C_D and C_L given the parameter distributions described above. This relationship incorporates the observations that mean $C_L = 0.85C_D$ and that the effective strength of an imposed fluid force is the same relative magnitude in the downstream and vertical directions. We also explore a range of simplified linear relationships between C_L and C_D as a further test of other possible covariations (or lack of covariation) between C_L and C_D (Text S1 and Figure S1). Our results show that the magnitude of variability in the critical velocity for grain motion is only mildly sensitive to the amount of covariation (or lack of covariation) between C_L and C_D, with positive correlation between C_L and C_D resulting in higher critical velocities and negative correlation producing similar mean values as uncorrelated with reduced variability (Figure S1).

Covariance between the other FBPs has not been clearly established, however, relationships between FBPs may be inferred. For example, a high μ value may be correlated with a low p_* value for a grain sitting well below the mean height of surrounding grains (Yager, Schmeeckle, & Badoux, 2018). Complex bed structure precludes us from making these direct assumptions however, as a grain with a high μ may represent a grain that is fully exposed to upstream flow (p_* value near unity), but is sitting in front of a larger grain. Other FBPs have no clear correlation; for example, ρ and ρ_s have not been explored as co-variable in other FBP, and there is no physical reasoning that variance in particle or fluid density would dramatically influence bed packing via μ or alter C_D or C_L, given they are independent inputs to equation 2 and 3, respectively. Lacking established relationships between FBPs such as μ and p_* we rely on the FBP distributions as currently measured to ensure we represent all probable bed configurations in the general case explored here. We recognize that refining the probable relationships between all FBPs is a clear avenue for future work, the results of which could be incorporated into the proposed framework.

2.4 Influence of force duration

Grain-mobilization thresholds depend on the product of the magnitude of the force and the duration over which it is applied, a quantity termed impulse (Diplas et al., 2008; Pähtz et al., 2020). By systematically modulating imposed force duration and magnitude, Diplas et al. (2008) showed that the magnitude of critical force rapidly increased as the force duration became vanishingly small, which concentrated most of the observed variability in the threshold of motion towards exceedingly small duration of force application. For short force durations, forces well above critical are needed to rapidly accelerate and move the grain out of its pocket before the force pulse ends. However, subsequent work demonstrated that high magnitude, exceedingly short duration forces rarely mobilize grains (Celik et al., 2013). Instead, mobilization commonly occurs by longer force pulses sustained at or near the threshold force, where the threshold force is determined by accounting for all body and surface forces acting on the grain (Figure 1a).

We assume that the force that results from all sampled combinations of FBP values are applied with sufficient duration to mobilize the grain and thus correspond to a unique grain-proximal critical velocity capable of initializing grain motion. This assumption should not be limiting if grain mobilization is dominated by longer-duration near-critical forces, as has been demonstrated in highly controlled impulse experiments that have yielded FBPs consistent with the distributions used here (Schmeeckle et al., 2007; Celik et al., 2013; Maniatis et al., 2020).

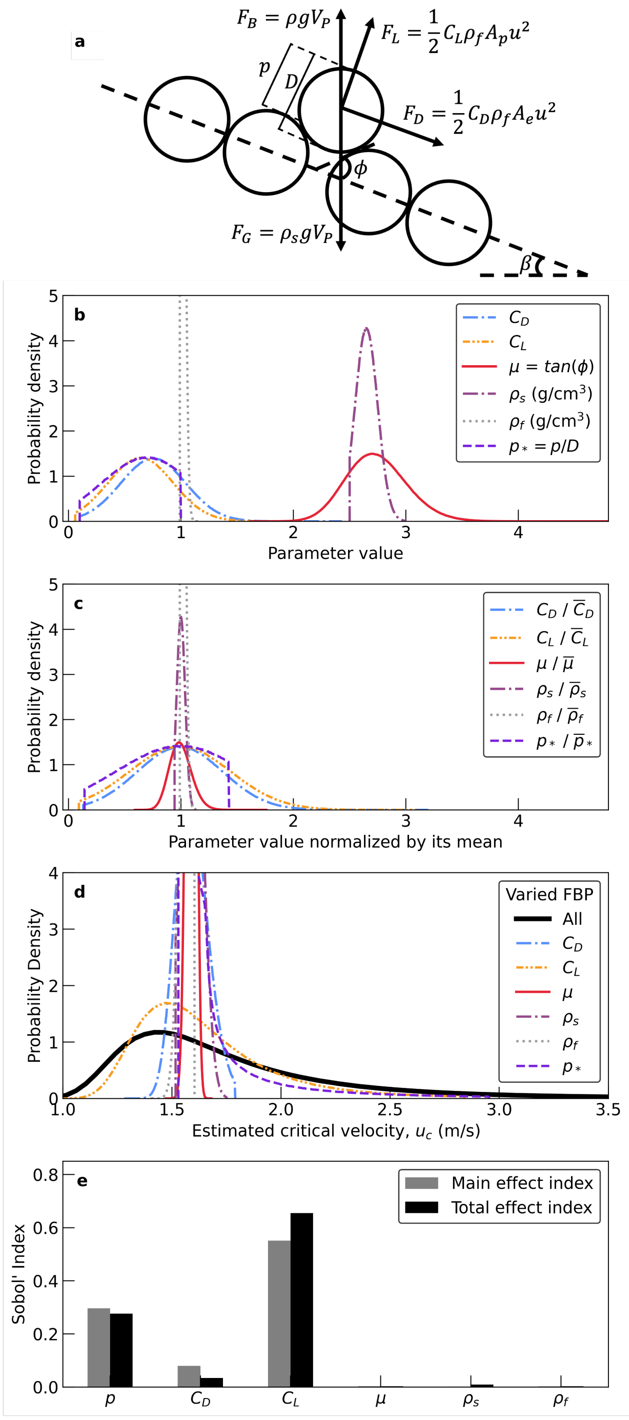

Figure 1. Variability of force-balance parameters (FBPs) and resulting sensitivity to these parameters. a) Schematic of forces acting on an individual grain (modified from Wiberg and Smith (1987)). b) FBP distributions for the general case given in Table 1. c) FBP distributions normalized by the mean value of each distribution. d) Estimated critical-velocity distributions for a 0.1 m diameter grain determined by varying all the parameters according to distributions shown in (a) (black solid line) compared to those resulting from varying each parameter individually while holding all others constant at their mean value (colored lines). e) Sobol' indices for each FBP indicating sensitivity of critical velocity to variability in FBPs. Light gray bars represent main effect indices and black bars represent total effect indices. In (b) - (d), y-axis limits truncate high-probability peaks of narrow distributions.

3 Sensitivity of critical velocity to variability in force-balance parameters

To determine which FBP distributions contribute most to the variability in incipient motion thresholds, we quantified the sensitivity of the expected critical velocity (Equation 10) to variability in each force-balance parameter using a one-at-a-time sensitivity analysis followed by a more formal global sensitivity analysis using Sobol' indices (Sobol, 2001). For the sensitivity analysis, we calculated the expected critical velocity distributions that resulted when only a single FBP was allowed to vary across its complete distribution, with all other FBPs held constant at their mean value. Sobol' global sensitivity indices provide estimates of the influence of individual or groups of variables on model outputs computed using Monte Carlo methods. We calculated Sobol' indices using Latin hypercube sampling and performed the global sensitivity analysis as implemented in the open-source software package `quoFEM` (McKenna et al., 2021). For this analysis, we used the distributions specified above (Figure 1b) and assumed near-perfect positive correlation between the lift and drag coefficients (correlation coefficient of 0.99). `quoFEM` allows users to wrap sensitivity analysis functionality around different analysis packages. In this case, we input a Python script describing the force-balance model as the input model for a global sensitivity analysis. We calculated both the main effect and total effect Sobol' indices to objectively assess the contributions of individual FBPs and FBP interactions to the overall variability in critical velocity predicted by our model. The main effect index provides a measure of an individual FBP's contribution to the total variance in the force-balance derived critical velocity, while the total effect index assesses variability added by a FBP due to its interaction with other FBPs.

For a given grain size, the one-at-a-time sensitivity analysis demonstrates that much of the observed variability in the critical velocity results from the lift coefficient and grain protrusion (Figure 1d) owing to the large variability of their distributions relative to their mean value (Figure 1c). This result does not indicate that other parameters such as μ and C_D are unimportant in setting the value of u_c; instead, it suggests that the variability in the FBP distributions for parameters such as μ and C_D do not contribute substantial variance to the expected u_c distribution.

The global sensitivity analysis using Sobol' indices confirms a large individual contribution to the variability in critical velocity from the lift coefficient and protrusion value. The lift coefficient accounts for 58% of u_c variability, while the protrusion and drag coefficient account for 32% and 9%, respectively. Fluid and sediment density combined account for $< 1\%$ of the u_c variability. Similarly, the effective friction coefficient accounts for $< 1\%$ of the u_c variability (Figure 1d). The main effect and total effect for all FBPs show similar patterns, though the total effect is greater than the main effect in all instances. This indicates that interaction between FBPs contributes some amount to u_c variance, though C_L and protrusion dominate the variance, whether individually or through interactions with other FBPs. If grain size is allowed to vary and all other FBPs are assumed to be uniformly distributed, grain size alone accounts for 68% of the variability in u_c and reduces the main effect for C_L to 27%. This highlights that grain size is the most dominant independent variable for formulating an incipient motion threshold (Figure S1b). Using uniform distributions instead of truncated normal distributions for FBPs results in only minor changes in sensitivity (Figure S2a), suggesting that the relative contributions of FBPs to u_c variability is somewhat independent of the assumed form of the FBP distributions.

Although C_L, C_D, and p are rarely quantified and not well known in most environments, our analysis offers insight into their respective influence on the variability of incipient motion. This sensitivity analysis suggests that further constraints on effective lift, drag and protrusion would decrease expected variability in the threshold of motion. However, if such variability in FBPs is characteristic of a site where one wants to predict sediment transport, then the large predicted variability is expected and should be used in incipient motion predictions.

4 Model-predicted distributions of incipient motion thresholds

To generate of critical-velocity distributions at incipient motion, we used a standard Monte Carlo method to propagate FBP variability through Equation 10 (Metropolis & Ulam, 1949). We drew 10^5 random samples from each respective FBP distribution to solve Equation 10 for 10^5 unique realizations of critical velocity for a given grain diameter. We repeated this Monte Carlo procedure across 1000 grain sizes linearly spaced from 0.002 m to 1 m diameter and stacked the probability density functions of critical velocity determined for each grain size to create a probability density map of critical velocity that varied with grain size and represents the expected variability of the threshold of motion (Figure 2a).

To compare with other incipient-motion thresholds, we convert these grain-proximal velocities into corresponding critical shear velocities (u_{*c}), critical shear stress (τ_c), and critical Shields stress (τ_c^*) (Figure 2b-d). These conversations are not straightforward, because u_c represents an instantaneous, point measurement, whereas u_{*c}, τ_c and τ_c^* are all spatially and temporally averaged quantities. However, given that u_*, τ_b and τ^* are arguably the most commonly used metrics to evaluate the threshold of motion (e.g., Wiberg & Smith, 1987; Lamb et al., 2008; Garcia, 2008; Williams et al., 2013; Deal et al., 2023), being able to relate the variability we calculate in u_c to these averaged quantities represents a potentially useful contribution. Our approach is two-fold. We first assume that the instantaneous u_c value is approximately equal to the velocity averaged over the height of a grain, u_a, at incipient motion. Second, we take the full distribution of u_c values, and calculate a corresponding distribution of critical shear velocity using a known velocity profile as described below (Lamb et al., 2017b). This is similar to the approach of Wiberg and Smith (1987) in converting a local-scale grain velocity to critical shear velocity using a velocity profile; however, we make the additional assumption that the instantaneous u_c value can be treated as a time-averaged quantity solely for the purpose of calculating variability in u_{*c}. This should result in a wider distribution of critical shear velocity, consistent with our conservative approach to estimate the maximum amount of variability in the threshold for motion. To convert to the corresponding u_{*c}, we also assume fully turbulent flow conditions such that the velocity profile is independent of Reynolds number and can be described by a modified logarithmic depth profile (Lamb et al., 2017b)

$$\frac{\overline{u}(z)}{u_*} = \frac{1}{k} \ln\left(1 + \frac{30z}{k_s}\right) \tag{11}$$

in which $\overline{u}(z)$ is the downstream velocity temporally averaged over turbulence and averaged laterally in space over variability in local bed roughness, z is distance above the bed, $k = 0.407$ is von Karman's constant, and k_s is the roughness layer height. From Equation 11 we calculate the velocity averaged over the height of a grain u_a. We assume that for a known grain size D, $u_a = u_c$ at incipient motion, given u_c represents the grain proximal downstream flow velocity in equation 10, we use this local velocity to solve for the corresponding u_{*c}, τ_c, and τ_c^* at incipient motion.

$$u_a = u_c = \frac{1}{z_2 - z_1} \int_{z_1}^{z_2} \overline{u}(z)\, dz = \frac{u_{*c}}{k(z_2 - z_1)} \int_{z_1}^{z_2} \ln\left(1 + \frac{30z}{k_s}\right) dz \tag{12}$$

$$u_c = \frac{u_{*c}}{(z_2 - z_1)k} \left(\left(\frac{k_s}{30} + z_2\right) \ln\left(\frac{30z_2}{k_s} + 1\right) - \left(\frac{k_s}{30} + z_1\right) \ln\left(\frac{30z_1}{k_s} + 1\right) - z_2 + z_1 \right) \tag{13}$$

$$u_{*c} = u_c(z_2 - z_1)k\left(\left(\frac{k_s}{30} + z_2\right)\ln\left(\frac{30z_2}{k_s} + 1\right) - \left(\frac{k_s}{30} + z_1\right)\ln\left(\frac{30z_1}{k_s} + 1\right) - z_2 + z_1\right)^{-1} \tag{14}$$

where z_1 and z_2 represent the vertical position of the bottom and top of the grain of interest, respectively.

We assume k_s ranges from $D \leq k_s \leq 6.1D$ and we allow the grain to sit anywhere within the roughness layer, that is, $k_s/30 + D \leq z_2 \leq k_s$ and set $z_1 = z_2 - D$ (Grant, 1997; López & Barragán, 2008). While other work has suggested narrow ranges in k_s (e.g., Lamb et al., 2017b), the large range used here ensures the widest possible distribution of critical velocities, consistent with our goal to quantify the maximum amount of potential variability in the force-balance approach.

For each Monte Carlo realization of Equation 10, we predicted the variability of critical shear velocity by randomly sampling values of k_s and z_2 from uniform distributions with limits as specified above, and we propagate those estimates through Equation 14, (Figure 2b). Assuming a constant k_s (e.g., $k_s = D$) reduces the variability by up to half relative to the case in which k_s varies within a uniform distribution (Figure S4). We calculated the variability for critical shear stress and critical Shields stress using

$$\tau_c = \rho u_{*c}^2 \tag{15}$$

and

$$\tau_c^* = \frac{\rho u_{*c}^2}{(\rho_s - \rho)gD} \tag{16}$$

The resulting distributions (Figure 2) highlight the expectation of large variability in incipient-motion thresholds given the measured variability in FBPs, but also show that well-defined high-density regions for each threshold can be characterized by the interquartile range (IQR) (Figure 2). We found that these high-density regions in the threshold u_c, u_{*c}, and τ_c distributions can be represented by a family of power laws fit between grain size and the respective flow parameter, with u_c and u_{*c} different only by their coefficient

$$\begin{gathered} u_c = m_c D^{0.5} \\ m_c = 5.21 \pm 0.91 \end{gathered} \tag{17}$$

$$\begin{gathered} u_{*c} = m_* D^{0.5} \\ m_* = 0.80 \pm 0.17. \end{gathered} \tag{18}$$

These power laws are based on the form of Equation 10, in which the FBP distributions reported in Table 1 result in a power law characterized by the reported m_c, while the power law exponent of 0.5 remains fixed. We solve for the best fit of τ_c by combining Equations 15 and 18, $\tau_c = \rho u_{*c}^2 = \rho m_*^2 (D^{0.5})^2$ which results in the linear relationship

$$\begin{gathered} \tau_c = m_\tau D \\ m_\tau = 648 \pm 285 \end{gathered} \tag{19}$$

where $m_\tau = \rho m_*^2$. Combining Equations 15, 16, and 19 yields $\tau_c^* = m_\tau/(\rho_s - \rho)g$, resulting in a constant τ_c^* value of

$$\tau_c^* = 0.040 \pm 0.018. \tag{20}$$

These functional relationships shown in Equations 17, 18, 19 and 20 predict a wide range of incipient motion thresholds, owing to our use of broad FBP distributions (Table 1) and thus should be valid, albeit with large expected variability, for spherical grains on Earth in low slope rivers. As we show below, if additional site-specific information is available (e.g., known sediment density, or a known and tighter range of drag coefficients), input FBP distributions can narrowed, resulting in reduced variability on the power law coefficients (m_c, m_*, m_τ) or τ_c^* estimate.

5 Comparison between model-predicted and empirically-observed incipient-motion thresholds and bedload flux

In this section we compare incipient-motion distributions predicted by our model to published data from flume experiments with controlled and limited parameter variability and field data with wider FBP ranges. We also use our model framework to show how variations in the incipient-motion threshold offer an explanation of the scatter in existing bedload flux measurements. These comparisons serve as concrete examples of how FBP distributions and resulting predictions of threshold distributions can be narrowed for a particular site of interest.

5.1 Comparison with large-replicate, single-grain entrainment flume experiments

We compared our model-predicted critical velocity distributions with published distributions measured in idealized flume experiments. Wu and Shih (2012) replicated two experiments of grain-entrainment (115 and 205 replicates, respectively) by placing spherical grains in idealized pocket geometries and measuring grain proximal velocities before and after initial grain motion using high-speed cameras and laser Doppler velocimetry. They found that the critical velocity at entrainment was not constant across replicates for an experiment, but instead took on a range of values well outside the uncertainty in their velocity measurements (Figure 3). The Wu and Shih (2012) experiments provide idealized data to test the accuracy of our force-balance model predictions in a fully controlled setting.

To compare our model predictions to the Wu and Shih (2012) data, we narrowed our input FBP distributions based on the experimental setup. We set the C_D distribution using the experimentally measured median velocity prior to entrainment based on the relationship between C_D and u_a measured by Schmeeckle et al. (2007) (Figure S3). Similarly, we decreased the mean and narrowed the range of μ to reflect the experimental pocket geometries and observed direction of initial sediment motion out of the pocket following Kirchner et al. (1990):

$$\mu = \tan(\phi) = \frac{\gamma}{\sqrt{(D_m/D_b)^2 + 2(D_m/D_b) - 1/3}} \tag{21}$$

where D_m is the diameter of the spherical particle being mobilized, D_b is the diameter of the spherical, uniform bed particles and γ is an empirical coefficient that is equal to $1/\sqrt{3}$ when the mobilizing particle pivots through the saddle between two downstream bed particles and is equal to $2/\sqrt{3}$ when the mobilizing particle pivots directly over one of the bed particles. This semi-empirical formulation uses a rolling initiation mechanism to calibrate the effective coefficient of friction. Although our balance of forces in Equation 1 is not based on a moment balance in which the rolling regime of particles are defined (e.g., Pähtz et al., 2020), Equation 21 allows us to characterize

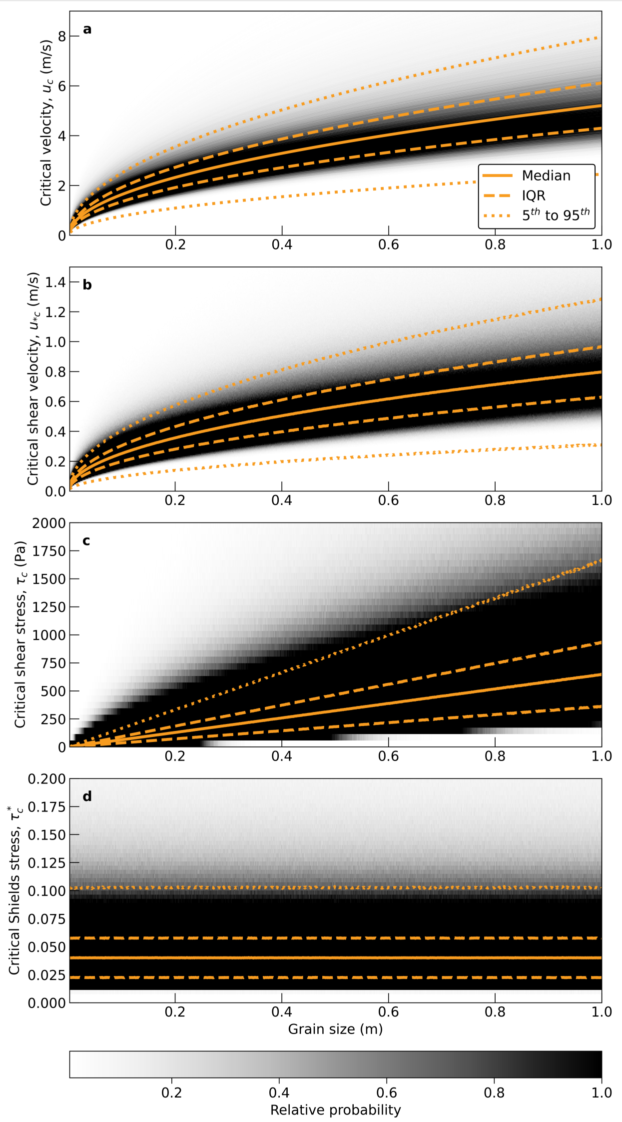

Figure 2. Probability density maps of critical flow properties calculated from force-balance parameter distributions specified in Table 1. Distribution of critical velocity (a), critical shear velocity (b), critical shear stress (c) and critical Shields stress (d) as a function of grain size found using a Monte Carlo Method to propagate variability of the force-balance parameters through a grain-scale force balance. Solid lines show power law fits to median values, long-dashed lines show the interquartile range and dotted lines show power law fit to the 5^{th} to 95^{th} percentile values. Black to gray shading shows density of values from the Monte Carlo method divided by the maximum density and is defined as the 'relative probability' in the colorbar.

an effective coefficient of friction to reflect geometric resistance to motion for a grain that will be mobilized via rolling, resulting in an inherently lower effective frictional resistance. For Wu and Shih (2012) Experiment 1, in which the mobilizing particle rotated through the saddle between two downstream particles, we set the mean of the ϕ distribution to 19 degrees with a range of 9 - 29 degrees to account for potential asphericity of particles and mobilization not directly through the saddle. In Wu and Shih (2012) Experiment 2, the grain was forced to exit over or oblique to a downstream particle and we used a mean μ of 35 degrees and a ϕ range of 25 - 45 degrees. We assumed a constant $p_* = 0.86$ for both experiments based on the position of the mobilized particle prior to entrainment. We held ρ and ρ_s constant to reflect the values from the study. Lacking additional constraints on C_L, we assumed a mean C_L = 0.19 (half the value of our general case) due to the low flow velocity, and the full C_L parameter distribution range from the most general case ($0.06 < C_L < 2$) (Table 1). Inputting these experiment-specific distributions into our Monte Carlo simulations resulted in a best fit $m_c = 2.54 \pm 0.29$ (median +/- interquartile range) for Experiment 1 (Figure 3a) and $m_c = 1.09 \pm 0.18$ for Experiment 2 (Figure 3b).

We found that the predicted critical velocity distributions using the simplified power law (Equation 17) and the updated m_c values (2.54 ± 0.29 for Experiment 1 and 1.09 ± 0.1 for Experiment 2) bound the range of velocities measured immediately before entrainment across all replicates (Figure 3a-b). Model-predicted critical velocities, in terms of both the mean and interquartile range, change in concert with the experimental configuration, owing to our use of experimental constraints on C_d, p, ρ, ρ_s, and ϕ. We interpret this agreement between our theoretical predictions and experimental observations as evidence that incorporating independently quantified variability in force-balance parameters allows accurate representation of the distribution of critical velocities at initiation of sediment motion. This supports our hypothesis that the variability observed in incipient motion data is encompassed within the expected variability associated with applicable FBP variability.

5.2 Comparison with field data

The comparison above represents idealized conditions where many replicates were used to quantify variability in the threshold velocity; however, such data are rarely available. We assessed the performance of the simplified family of power laws in less idealized conditions by comparing model predictions to field and flume data spanning a variety of incipient motion observation techniques, inferred flow conditions, bed packing and grain size.

5.2.1 Comparison with field measurements of paired incipient motion and grain-scale critical velocity

Helley (1969) conducted a unique field experiment placing natural grains (up to 0.52 m in diameter) on a natural riverbed at low flow and recorded the incipient motion of these grains with concurrent flow depth. This allowed a threshold grain-scale flow velocity to be determined using a calibrated stage-velocity relation. To our knowledge, this is the only incipient motion field data with constraints on grain-scale flow velocity, and is thus the best suited field data to test our model. We used reported grain properties (the three primary axes, sediment density and particle volume) and the inferred relative position within the bed to constrain FBP distributions. Owing to the nature of grain placement on top of the natural sediment bed, we assumed low frictional resistance from bed packing and grain burial and therefore used a μ distribution (mean $\phi = 40°$, standard deviation = $15°$) which minimizes the contribution of bed packing to the effective friction angle (Kirchner et al., 1990). We assumed grains have high protrusion ($p_* = 0.9 \pm 0.2$). All other FBP distributions followed the distributions

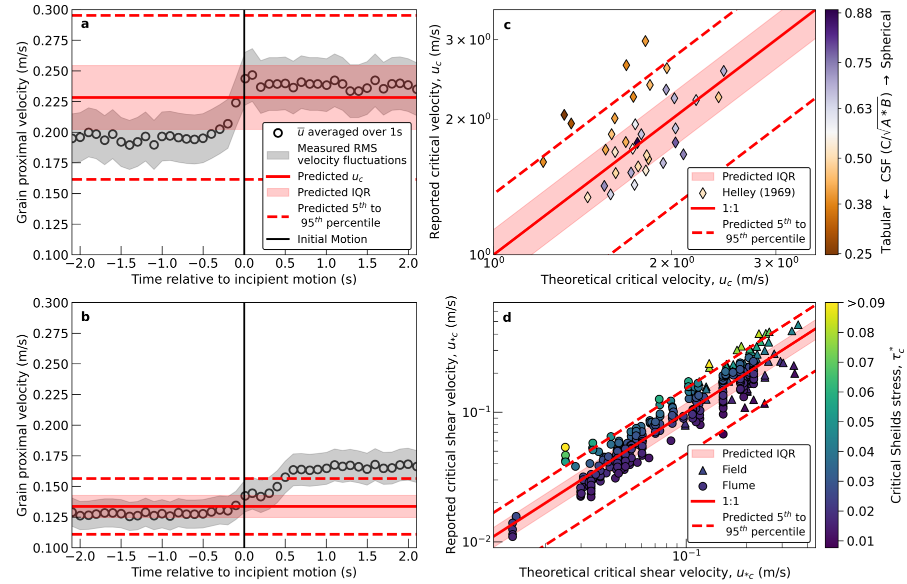

Figure 3. Comparison between model-predicted (red lines and red shading) and experimentally observed (various point symbols) flow conditions at incipient motion. (a and b) Downstream component of the grain-proximal velocity measured using laser Doppler velocimetry by Wu and Shih (2012) in two different bed packing configurations with different grain densities. Open circles indicate mean velocity measurements from all replicate experiments averaged over 0.1 s intervals. Grey shading spans the root-mean-square error of velocity fluctuations measured across all replicate experiments. (c) Observed velocity at incipient motion by Helley (1969) from Blue Creek, CA against expected theoretical critical velocity with points colored by their respective Cory Shape Factor (CSF), where A is the long axis, B is the intermediate axis and C is the short axis. Tabular particles that do not conform to the assumptions used to estimate critical velocity have small CSF, whereas more spherical particles have high CSF. (d) Reported critical shear velocity from compilation of field (triangles) and flume (circles) data against expected theoretical critical shear velocity with point color representing the reported critical Shields stress for data referred to in Section 6.2.2. For all plots, solid lines show the power law for median values, dashed lines show power law for the 5^{th} and 95^{th} percentile values, and colored patches span the interquartile range estimated using the reported grain size.

specified in Table 1, these broad values and the physical constraints described above resulted in a best fit m_c value of 3.77 ± 0.31.

The resulting comparison between modeled and observed critical velocities shows that the predicted threshold velocity and the interquartile range of uncertainty encompass a majority of the observations for grains that are approximately spherical (Figure 3c). Some of the reported velocities, particularly for tabular grains, are higher than the interquartile range estimate from our force-balance predictions (Figure 3c), potentially due to the fact that we use distributions of drag and lift coefficients for approximately spherical grains, which may systematically overestimate drag and lift coefficients for tabular grains. We interpret the tight correspondence between observed and predicted critical velocities and the degree to which a majority of approximately spherical grains fall within our predicted interquartile range as a second positive test of our hypothesis that incorporating variability in FBP offers a reasonable estimate of the critical velocity and variability in that velocity. This second positive test adds additional credibility to our hypothesis because it was carried out in a natural setting and with significantly larger grain sizes (up to $D = 0.52$ m) relative to the previous laboratory comparison.

5.2.2 Comparison with field and flume data of incipient motion with reach-averaged critical shear velocity

In practice, most field and laboratory data do not allow a direct estimate of grain-scale flow velocity as in the Wu and Shih (2012) and Helley (1969) datasets. We tested the ability of our force-balance model to capture variability in incipient motion using data more commonly collected in the lab and field data. Specifically, we used a large compilation of estimated critical shear velocity at incipient motion from flume experiments and field observations (Aguirre-Pe, 1975; Andrews, 1994; Buffington & Montgomery, 1997; Andrews, 2000; Shvidchenko et al., 2001; Church & Hassan, 2002; Mueller et al., 2005; Whitaker & Potts, 2007; Scheingross et al., 2013; Prancevic et al., 2014). Owing to the diversity of field and flume data included in this compilation, we predicted critical velocities using the most general FBP distributions in Table 1. We assumed a roughness layer height of $k_s = D$ for Equation 14 to maintain consistency with assumptions in Buffington and Montgomery (1997), this is likely an underestimate of the true roughness layer height which may result in overestimates of u_{*c}. We filtered the incipient motion data to include observations with slopes $< 5\%$ and $D_{50} > 0.001$ m, set by the assumptions of our methodology. We observe that 61% of the flume data fall within the interquartile range of our model predictions, and 95% of flume data fall within the 5 to 95% confidence interval (Figure 3d). Field data shows a similar consistency with 39% and 90% falling within the IQR and 5 to 95% confidence interval, respectively. We interpret this as additional strong support of our hypothesis that incorporating known variability in FBP can explain observed variability in thresholds at incipient motion.

While the majority of data fall within our predicted variability bounds, the predicted critical shear velocity is biased high (i.e., a majority of points plot below the one-to-one line). One potential explanation for this bias is the assumption of spherical grains which may overestimate grain volume, thus requiring a higher estimated critical shear velocity to mobilize the grains than observed. An additional source of variability not included in our analysis is the variability that might result from mixing measurement techniques and definitions for incipient motion, which in the compilation include defining a non-zero sediment flux, visual observation of initial to full bed mobility, empirical competence and theoretical estimates for a given flow condition (Buffington & Montgomery, 1997). Despite this additional variability, we are able to estimate the range of threshold conditions observed across decades of incipient motion studies through incorporating expected variability in the forces controlling entrainment.

5.3 Estimating expected variability in bedload flux

Bedload flux is characterized by large fluctuations, particularly when flow conditions are near the threshold of motion (e.g., Figure 4 and Ancey et al. (2008)). Following from the early work of Einstein (1950), there has been renewed interest in stochastic formulations to predict bedload flux and observed variability (Seminara et al., 2002; Ancey, 2010; Foufoula-Georgiou & Stark, 2010; Turowski, 2010; Furbish et al., 2012; Ancey & Heyman, 2014; Fathel et al., 2015; Heyman et al., 2016; Ancey & Pascal, 2020; Benavides et al., 2022; Pierce et al., 2022). Despite these attempts that offer new theory to estimate and explain observed variability in bedload flux, empirical, deterministic formulations are still the most common approach to quantifying bedload flux (e.g., Meyer-Peter & Müller, 1948; Fernandez Luque & Van Beek, 1976; Wong & Parker, 2006). Here we present a method that incorporates the expected variability in incipient motion developed above, and that includes variability in fluid stress and bed configuration, to offer bounds of expected variability on commonly applied deterministic bedload flux formulations.

The most commonly used formulae to estimate bedload transport take the form of

$$q_* = a(\tau^* - \tau_c^*)^b \tag{22}$$

where $q_* = q_s/(RgD^3)$ is a non-dimensional bedload flux per unit width, q_s is the volumetric bedload flux per unit width, $R = (\rho_s - \rho)/\rho$ and a and b are empirically-derived constants (e.g., Meyer-Peter & Müller, 1948; Fernandez Luque & Van Beek, 1976; Wong & Parker, 2006). Inspection of Equation 22 highlights that small variation in τ_c^* can lead to large variations in bedload flux estimates, due to the non-linear dependence of sediment flux on excess Shield stress (τ^* - τ_c^*).

To illustrate how variability in the threshold of motion can be propagated to estimate expected variability in sediment flux, we used our framework to add variability to the well-established Wong and Parker (2006) bedload flux empirical relationship,

$$q_* = 4.93(\tau^* - \tau_c^*)^{1.60} \tag{23}$$

where Wong and Parker (2006) set $\tau_c^* = 0.0470$ based on a best fit to data. We use our Monte Carlo method to assess variability around $\tau_c^* = 0.0470$. To reproduce this τ_c^* value, we assume all FBPs follow the most general distributions from Table 1, but we set mean $p_* = 0.3$ to increase τ_c^* from our estimate of 0.040 to the 0.047 best fit from (Wong & Parker, 2006). This results in an interquartile range of τ_c^* values ranging from $0.025 < \tau_c^* < 0.69$, or $\tau_c^* = 0.047$ +/- 0.022.

The expected variability around the Wong and Parker (2006) relationship derived from our force-balance framework accounts for 89% of the observed variability in the bedload flux measurements on which the Wong and Parker relationship was originally calibrated Figure 4. One potential reason our variability estimates encompass 89% of the data, even though it is based on the interquartile range of expected τ_c^* values, is because we used the full range of FBP distributions in Table 1. This variability could be reduced if FBP measurements were available for the sediment flux data, in which case we would expect the predicted variability to encompass closer to 50% of the data. Regardless, we interpret the fact that variability from our framework encompasses the observed data to suggest that variability in incipient motion from force-balance parameters can be used to better constrain expected variation in sediment flux.

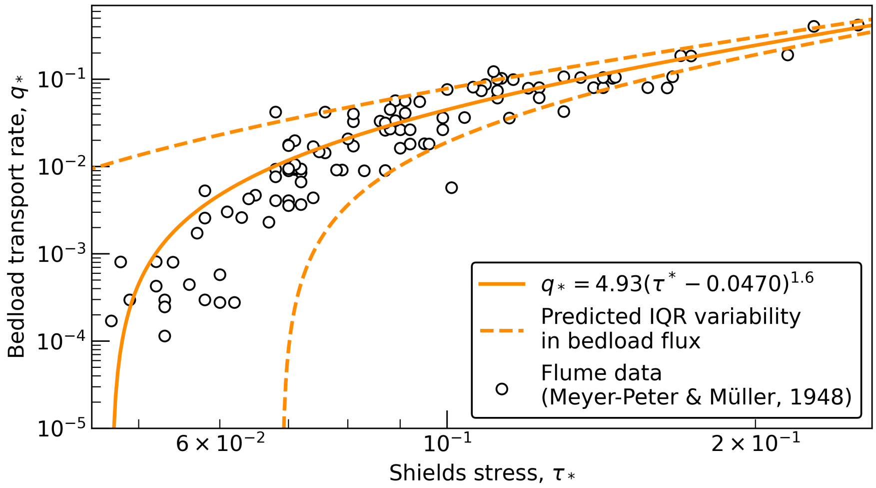

Figure 4. Comparison of flume-measured bedload flux (Meyer-Peter & Müller, 1948) with the Wong and Parker (2006) empirical fit. Interquartile range of variability on τ_c^* predicted using the framework developed here (see text for details). q_* is the dimensionless volume bedload flux per unit width and τ^* is the Shields stress.

6 Discussion

Our results demonstrate that the magnitude of scatter observed in flow metrics at that time of incipient motion is predictable and is encompassed within the variability expected from independently quantified and site-specific distributions of force-balance parameters (Figure 3). Furthermore, our results provide a simple method to constrain expected variability in the threshold of motion using a power law function, $u_c = m_c D^{0.5}$, where the power law coefficient, m_c, changes to encompass expected FBP variability.

The power law relationship between critical velocity and sediment size has been observed empirically for centuries (Brahms, 1753; Leliavsky, 1955; Strand, 1973) and is a natural result when formulating a grain-scale force balance to solve for a critical velocity (Wiberg & Smith, 1987, Equation 10). The novel result found here is that the degree of variation on the power law coefficient is predictable based on independent laboratory and field measurements of parameters used to close the force balance (Figure 3), and that this variability is most often dominated by variability in the distributions of effective lift, drag and protrusion (Figure 1d). When the expected variability in force-balance parameters is explicitly incorporated, the resulting threshold of motion distributions show that substantial deviations from commonly assumed values (e.g., τ_c^* = 0.045) are possible (Figure 2). The modeling framework presented here allows the observed FBP variability to be easily propagated to estimated the expected variability of critical velocity, critical shear stress or critical Shields stress allowing for more robust, even if uncertain, estimates of incipient-motion thresholds.

While our analysis used a Monte Carlo method to propagate FBP variability to variability in incipient motion, we show that the threshold of motion can be described by a family of easy-to-use power laws describing both the mean and variability about the mean for incipient motion as a function of grain size. To aid in rapid calculation of expected variability in incipient motion thresholds we compiled a table of power law fit coefficients (m, i.e., m_c, m_*, m_τ, and τ_c^*) with associated variability that span flow, grain and bed conditions that are likely to be encountered on Earth and other planetary bodies (Table S1). If little information is known about the site and flows expected there, the most variable m values presented in Section 4 should provide robust estimates that incorporate the possibility of broad variability due to the lack of site-specific values for FBPs. If it is possible to inform the expected distribution of flow velocities, bed conditions, grain or fluid properties, then one can better constrain the variability in the m value selected and reduce the expected variability in incipient motion.

To facilitate easy selection of m for the most readily constrained bed properties of ϕ and p_* we compiled m values and variability by varying mean values of ϕ and p_* (Figure 5). These results highlight how the expected m_c, m_*, m_τ, and τ_c^* and associated variability change when shifting the mean of two FBPs from those presented in Table 1. These plots also highlight that changing mean parameter values, such as the effective friction coefficient $\mu = tan(\phi)$, can have a large impact on the expected critical velocity (as seen by the notable increases in m as a function of ϕ in Figure 5). This is despite μ being one of the smaller contributors to the expected variance in u_c distributions (Figure 1d) owing to the relatively small variance relative to the mean found in many field-measured ϕ distributions (e.g., Hodge et al., 2013; Prancevic & Lamb, 2015). This variability in the respective m values also informs our intuition of how small changes in bed configuration, expressed through ϕ and p_*, may influence incipient-motion thresholds and how these parameters may change as a fluvial system evolves (Masteller et al., 2019).

Our results highlight that expected variability in incipient sediment motion can be related to FBP variability. As more FBP distributions become available, we will be able to decrease the variability in our predictions of the onset of incipient motion for particular flow and bed conditions. The results from our global sensitivity analysis highlight that variability in the distributions of effective lift, drag and protrusion are the current largest contributors to variability in critical velocity (Figure 1), and hence are obvious targets for further study. However, further investigation into FBP distributions might reveal that substantial variation in some FBPs is to be expected in certain flow and bed conditions such that there will be fundamental limits as to how small variability in critical velocity thresholds could become. For example, if future investigations continue to show broad distributions in C_D, the distributions of critical velocity cannot become tighter than the variance contributed by the C_D distribution.

While the framework presented here represents a simple and straightforward way to account for variability in incipient motion, additional improvement could be made by substituting our descriptions of drag, lift, and frictional forces for expressions that explicitly account for different mechanisms promoting or resisting grain entrainment, as opposed to lumping the effects of multiple mechanisms into simplified expressions with effective coefficients. The simplified expressions used here rely on effective parameters, making it difficult to directly attribute threshold variability to measurable flow, grain or bed properties. For example, Schmeeckle et al. (2007) presents a derivation of the nominal drag force acting on a stationary particle that could be implemented in our framework to more closely scrutinize the effect of 3D grain-fluid interactions for grain entrainment in laminar, transitional, or turbulent flow. The lift force, however, is a more complicated component to implement as there is a lack of general agreement on how to properly quantify or estimate the influence of lift on grain entrainment (as discussed in Dey et al. (2020)); further work is required to refine the quantitative description of lift before incorporation into the framework presented here. Recent work from Yager, Schmeeckle, and Badoux (2018) proposes three separate equations, each with unique measurable bed and grain parameters to explicitly describe resisting forces resulting from pocket geometry, grain burial, and bed packing. Incorporating these equations, as opposed to lumping all effects into a single simplified effective friction rule (as we have done), would be a clear improvement once sufficient measurements

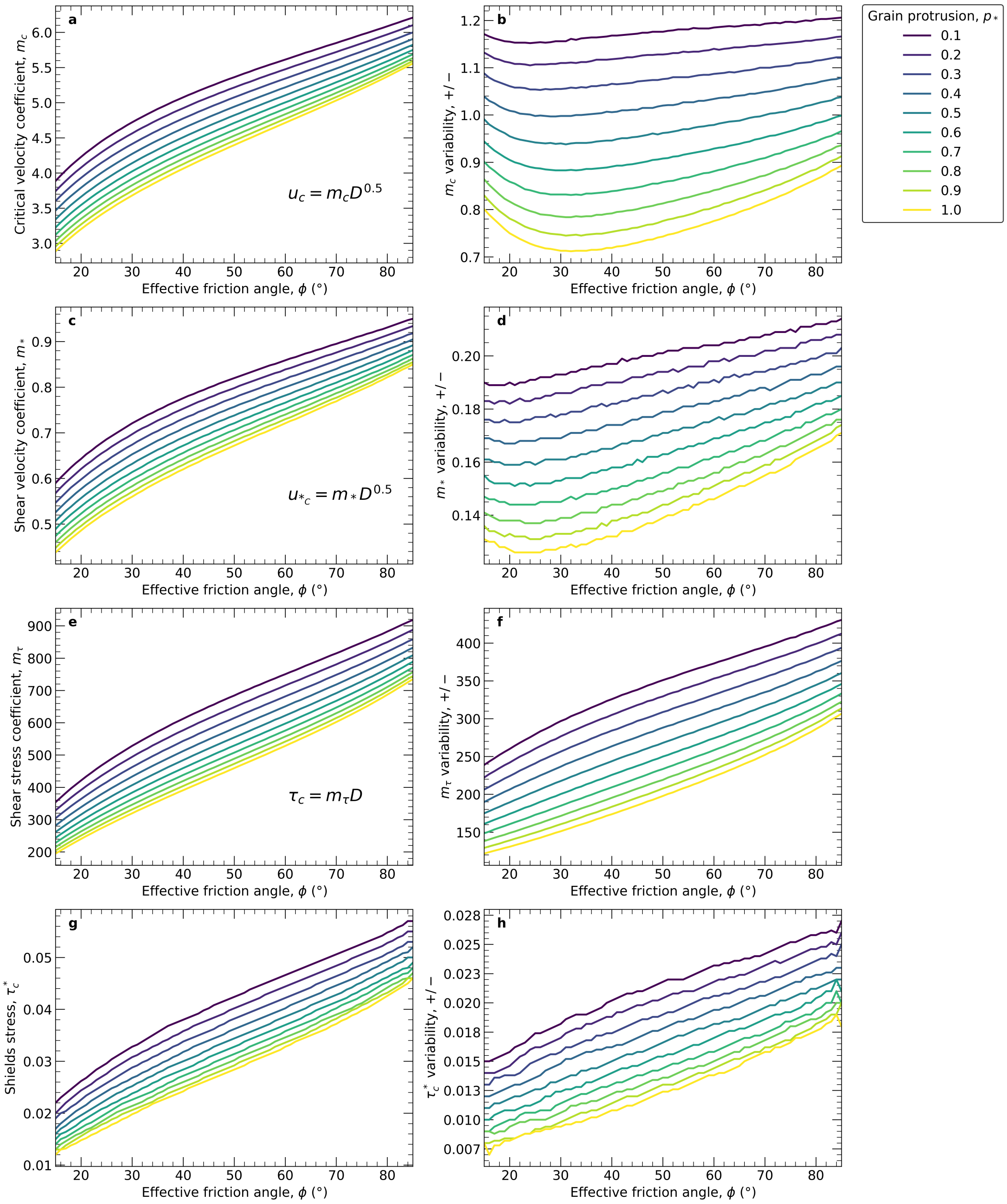

Figure 5. Best-fit power law coefficients (i.e., m_c, m_*, m_τ, and τ_c^*) as a result of altering the assumed mean of the effective friction angle (ϕ) and the relative grain protrusion (p_*). Best-fit power law coefficients and associated variability (IQR, $+/-$) for (a and b) critical velocity (u_c), (c and d) critical shear velocity (u_{*c}), and (e and f) critical shear stress (τ_c). (g and h) critical Shields stress (τ_c^*) and associated variability. m_c, m_*, m_τ and τ_c^* displayed as a function of mean ϕ and colored by mean p_*. All other force-balance parameter distributions are as specified in Table 1.

have been made. Even though our investigation into potential impacts of covariability between parameters revealed only second-order importance (Figure S1), explicitly accounting for co-variability in FBPs such as is probable between C_D and C_L for a given bed packing or grain protrusion scenario may lead to more accurate representations of threshold distributions (Schmeeckle et al., 2007; Dwivedi et al., 2011). As additional field and laboratory measurements become available, substituting these refined parameter distributions into the current framework should increase the robustness of output threshold distributions as well as increase the ability to select more accurate FBP distributions based on independent field and laboratory measurements.

7 Conclusions

Our results demonstrate that the magnitude of scatter observed in incipient motion is predictable and is encompassed within the variability expected from independently quantified and site-specific variability in the force-balance parameters. This threshold of motion can be described by a family of easy-to-use power laws describing both the mean and variability about the mean for incipient motion as a function of grain size. The degree of variation on the power law coefficient is predictable based on independent measurements of force-balance parameters and that this variability is most often dominated by variability in the distributions of effective lift, drag and protrusion. As more force-balance parameter distributions become available, we will be able to make more accurate estimates of expected variability at the onset of incipient motion for particular flow and bed conditions. When such constraints are lacking, using broadly applicable force-balance distributions accurately characterizes variability observed across diverse field settings. Thus, while variability in incipient sediment motion will always persist, having a means of assessing that variability should allow for more robust estimates of sediment transport across environmental conditions and planetary bodies.

Acknowledgements

We thank Jeff Prancevic for sharing compiled incipient motion data, Fu-Chun Wu and Wu-Rong Shih for sharing incipient motion flume data, Elowyn Yager for sharing in-situ observations of relative protrusion, and Editor Ton Hoitink, Associate Editor Christophe Ancey and three anonymous reviewers for comments that improved the quality of this manuscript. This work was supported by NASA awards 80NSSC19K0165 and 80NSSC20K1343 to SWM.

Open Research

The data and codes associated with this manuscript are available through Figshare: `https://doi.org/10.6084/m9.figshare.22266187` (Feehan et al., 2023). We used version 6.14 of Dakota for the sensitivity analysis. The application was built from source code available from the Dakota Git repository available at `https://dakota.sandia.gov/` using repository revision 382229e53 (McKenna et al., 2021).

References

Aguirre-Pe, J. (1975). Incipient erosion in high gradient open channel flow with artificial roughness elements. *Proc. 16th Congr. Int. Assoc. Hydraul. Res. San Paulo Brazil*(2), 137–180. (Aguirre-Pe, J. (1975). Incipient erosion in high gradient open channel flow with artificial roughness elements. Proc. 16th Congr. Int. Assoc. Hydraul. Res. San Paulo Brazil, 2, 137-180.)

Ali, S. Z., & Dey, S. (2016, July). Hydrodynamics of sediment threshold. *Physics* *of Fluids*, *28*(7), 075103. Retrieved 2023-02-01, from http://aip.scitation.org/doi/10.1063/1.4955103 doi: 10.1063/1.4955103

Ali, S. Z., & Dey, S. (2018, April). Impact of phenomenological theory of turbulence on pragmatic approach to fluvial hydraulics. *Physics of Fluids*, *30*(4), 045105. Retrieved 2023-02-03, from http://aip.scitation.org/doi/10.1063/1.5025218 doi: 10.1063/1.5025218

Ancey, C. (2010, June). Stochastic modeling in sediment dynamics: Exner equation for planar bed incipient bed load transport conditions: STOCHASTIC MODELING IN SEDIMENT DYNAMICS. *Journal of Geophysical Research: Earth Surface*, *115*(F2). Retrieved 2023-07-29, from http://doi.wiley.com/10.1029/2009JF001260 doi: 10.1029/2009JF001260

Ancey, C., Davison, A. C., Böhm, T., Jodeau, M., & Frey, P. (2008, January). Entrainment and motion of coarse particles in a shallow water stream down a steep slope. *Journal of Fluid Mechanics*, *595*, 83–114. Retrieved 2023-07-29, from https://www.cambridge.org/core/product/identifier/S0022112007008774/type/journal_article doi: 10.1017/S0022112007008774

Ancey, C., & Heyman, J. (2014, April). A microstructural approach to bed load transport: mean behaviour and fluctuations of particle transport rates. *Journal of Fluid Mechanics*, *744*, 129–168. Retrieved 2023-07-29, from https://www.cambridge.org/core/product/identifier/S0022112014000743/type/journal_article doi: 10.1017/jfm.2014.74

Ancey, C., & Pascal, I. (2020, July). Estimating Mean Bedload Transport Rates and Their Uncertainty. *Journal of Geophysical Research: Earth Surface*, *125*(7). Retrieved 2023-07-21, from https://onlinelibrary.wiley.com/doi/10.1029/2020JF005534 doi: 10.1029/2020JF005534

Andrews, E. D. (1994, July). Marginal bed load transport in a gravel bed stream, Sagehen Creek, California. *Water Resources Research*, *30*(7), 2241–2250. Retrieved 2022-02-20, from http://doi.wiley.com/10.1029/94WR00553 doi: 10.1029/94WR00553

Andrews, E. D. (2000, February). Bed material transport in the Virgin River, Utah. *Water Resources Research*, *36*(2), 585–596. Retrieved 2022-02-20, from http://doi.wiley.com/10.1029/1999WR900257 doi: 10.1029/1999WR900257

Baker, V. R. (2002, March). The study of superfloods. *Science*, *295*(5564), 2379–2380. Retrieved 2021-11-12, from https://www.science.org/doi/10.1126/science.1068448 doi: 10.1126/science.1068448

Benavides, S. J., Deal, E., Rushlow, M., Venditti, J. G., Zhang, Q., Kamrin, K., & Perron, J. T. (2022, March). The Impact of Intermittency on Bed Load Sediment Transport. *Geophysical Research Letters*, *49*(5). Retrieved 2023-07-21, from https://onlinelibrary.wiley.com/doi/10.1029/2021GL096088 doi: 10.1029/2021GL096088

Booth, A. M., Hurley, R., Lamb, M. P., & Andrade, J. E. (2014, December). Force chains as the link between particle and bulk friction angles in granular material: Granular force chains and friction angle. *Geophysical Research Letters*, *41*(24), 8862–8869. Retrieved 2021-11-12, from http://doi.wiley.com/10.1002/2014GL061981 doi: 10.1002/2014GL061981

Brahms, A. (1753). Anfangsgrunde der deich und wasserbaukunst Aurich.

Bridge, J. S., & Bennett, S. J. (1992, February). A model for the entrainment and transport of sediment grains of mixed sizes, shapes, and densities. *Water Resources Research*, *28*(2), 337–363. Retrieved 2023-03-03, from http://doi.wiley.com/10.1029/91WR02570 doi: 10.1029/91WR02570

Buffington, J. M., & Montgomery, D. R. (1997, August). A systematic analysis of eight decades of incipient motion studies, with special reference to gravel-bedded rivers. *Water Resources Research*, *33*(8), 1993–2029. Retrieved 2021-11-12, from http://doi.wiley.com/10.1029/96WR03190 doi: 10.1029/96WR03190

Celik, A. O., Diplas, P., & Dancey, C. L. (2013, April). Instantaneous turbulent forces and impulse on a rough bed: Implications for initiation of bed material movement: Instantaneous turbulent forces and impulse on a rough bed. *Water Resources Research*, *49*(4), 2213–2227. Retrieved 2022-04-06, from http://doi.wiley.com/10.1002/wrcr.20210 doi: 10.1002/wrcr.20210

Chiew, Y. M., & Parker, G. (1995). Reply to discussion of: Incipient sediment motion on non-horizontal slopes. *J. of Hydraulic Research*, *IAHR*(33(5)), 729–730.

Christensen, B. A. (1995, September). Incipient Sediment Motion On Non-Horizontal Slopes. *Journal of Hydraulic Research*, *33*(5), 725–730. Retrieved from https://doi.org/10.1080/00221689509498569 (Publisher: Taylor & Francis) doi: 10.1080/00221689509498569

Church, M., & Hassan, M. A. (2002, November). Mobility of bed material in Harris Creek. *Water Resources Research*, *38*(11), 19–1–19–12. Retrieved 2022-02-20, from http://doi.wiley.com/10.1029/2001WR000753 doi: 10.1029/2001WR000753

Church, M., Hassan, M. A., & Wolcott, J. F. (1998, November). Stabilizing self-organized structures in gravel-bed stream channels: Field and experimental observations. *Water Resources Research*, *34*(11), 3169–3179. Retrieved 2021-11-12, from http://doi.wiley.com/10.1029/98WR00484 doi: 10.1029/98WR00484

Deal, E., Venditti, J. G., Benavides, S. J., Bradley, R., Zhang, Q., Kamrin, K., & Perron, J. T. (2023, January). Grain shape effects in bed load sediment transport. *Nature*, *613*(7943), 298–302. Retrieved 2023-02-01, from https://www.nature.com/articles/s41586-022-05564-6 doi: 10.1038/s41586-022-05564-6

Dey, S., & Ali, S. Z. (2017a, November). Mechanics of Sediment Transport: Particle Scale of Entrainment to Continuum Scale of Bedload Flux. *Journal of Engineering Mechanics*, *143*(11), 04017127. Retrieved 2023-02-03, from https://ascelibrary.org/doi/10.1061/%28ASCE%29EM.1943-7889.0001343 doi: 10.1061/(ASCE)EM.1943-7889.0001343

Dey, S., & Ali, S. Z. (2017b, May). Stochastic mechanics of loose boundary particle transport in turbulent flow. *Physics of Fluids*, *29*(5), 055103. Retrieved 2023-02-03, from http://aip.scitation.org/doi/10.1063/1.4984042 doi: 10.1063/1.4984042

Dey, S., & Ali, S. Z. (2018, June). Review Article: Advances in modeling of bed particle entrainment sheared by turbulent flow. *Physics of Fluids*, *30*(6), 061301. Retrieved 2023-02-03, from http://aip.scitation.org/doi/10.1063/1.5030458 doi: 10.1063/1.5030458

Dey, S., Ali, S. Z., & Padhi, E. (2020, June). Hydrodynamic Lift on Sediment Particles at Entrainment: Present Status and Its Prospect. *Journal of Hydraulic Engineering*, *146*(6), 03120001. Retrieved 2023-04-15, from https://ascelibrary.org/doi/10.1061/%28ASCE%29HY.1943-7900.0001751 doi: 10.1061/(ASCE)HY.1943-7900.0001751

Diplas, P., Dancey, C. L., Celik, A. O., Valyrakis, M., Greer, K., & Akar, T. (2008, October). The Role of Impulse on the Initiation of Particle Movement Under Turbulent Flow Conditions. *Science*, *322*(5902), 717–720. Retrieved 2021-11-12, from https://www.science.org/doi/10.1126/science.1158954 doi: 10.1126/science.1158954

Dwivedi, A., Melville, B. W., Shamseldin, A. Y., & Guha, T. K. (2011, June). Analysis of hydrodynamic lift on a bed sediment particle: ANALYSIS OF LIFT ON A SEDIMENT PARTICLE. *Journal of Geophysical Research: Earth Surface*, *116*(F2). Retrieved 2023-02-03, from http://doi.wiley.com/10.1029/

2009JF001584 doi: 10.1029/2009JF001584
Einstein, H. A. (1950). The Bed-Load Function for Sediment Transportation in Open Channel Flows. *United States Department of Agriculture*, *No. 1026*.
Einstein, H. A., & El-Samni, E.-S. A. (1949, July). Hydrodynamic Forces on a Rough Wall. *Reviews of Modern Physics*, *21*(3), 520–524. Retrieved 2021-11-12, from https://link.aps.org/doi/10.1103/RevModPhys.21.520 doi: 10.1103/RevModPhys.21.520
Fathel, S. L., Furbish, D. J., & Schmeeckle, M. W. (2015, November). Experimental evidence of statistical ensemble behavior in bed load sediment transport. *Journal of Geophysical Research: Earth Surface*, *120*(11), 2298–2317. Retrieved 2023-07-29, from https://onlinelibrary.wiley.com/doi/10.1002/2015JF003552 doi: 10.1002/2015JF003552
Feehan, S. A., McCoy, S. W., Scheingross, J. S., & Gardner, M. H. (2023). *Quantifying variability of incipient-motion thresholds in gravel-bedded rivers using a grain-scale force-balance model: Software and Dataset.* figshare. Retrieved from https://doi.org/10.6084/m9.figshare.22266187
Ferguson, R., & Church, M. (2004, November). A Simple Universal Equation for Grain Settling Velocity. *Journal of Sedimentary Research*, *74*(6), 933–937. Retrieved 2021-11-12, from https://pubs.geoscienceworld.org/jsedres/article/74/6/933-937/99413 doi: 10.1306/051204740933
Fernandez Luque, R., & Van Beek, R. (1976, April). Erosion And Transport Of Bed-Load Sediment. *Journal of Hydraulic Research*, *14*(2), 127–144. Retrieved 2021-11-12, from http://www.tandfonline.com/doi/abs/10.1080/00221687609499677 doi: 10.1080/00221687609499677
Foufoula-Georgiou, E., & Stark, C. (2010, June). Introduction to special section on Stochastic Transport and Emergent Scaling on Earth's Surface: Rethinking geomorphic transport-Stochastic theories, broad scales of motion and nonlocality: INTRODUCTION. *Journal of Geophysical Research: Earth Surface*, *115*(F2). Retrieved 2023-07-29, from http://doi.wiley.com/10.1029/2010JF001661 doi: 10.1029/2010JF001661
Furbish, D. J., Haff, P. K., Roseberry, J. C., & Schmeeckle, M. W. (2012, September). A probabilistic description of the bed load sediment flux: 1. Theory: BED LOAD FLUX, 1. *Journal of Geophysical Research: Earth Surface*, *117*(F3), n/a–n/a. Retrieved 2023-07-21, from http://doi.wiley.com/10.1029/2012JF002352 doi: 10.1029/2012JF002352
Garcia, M. (Ed.). (2008). *Sedimentation Engineering: Processes, Measurements, Modeling, and Practice.* Reston, VA: American Society of Civil Engineers. Retrieved 2023-02-19, from http://ascelibrary.org/doi/book/10.1061/9780784408148 doi: 10.1061/9780784408148
Gessler, J. (1971). Beginning and ceasing of sediment motion. *River mechanics*, *1(1)*(7-1). (Gessler, J. (1971). Beginning and ceasing of sediment motion. River mechanics, 1(1), 7-1.)
Grant, G. E. (1997, February). Critical flow constrains flow hydraulics in mobile-bed streams: A new hypothesis. *Water Resources Research*, *33*(2), 349–358. Retrieved 2022-04-13, from http://doi.wiley.com/10.1029/96WR03134 doi: 10.1029/96WR03134
Grass, A. J. (1970, March). Initial Instability of Fine Bed Sand. *Journal of the Hydraulics Division*, *96*(3), 619–632. Retrieved 2021-11-12, from http://ascelibrary.org/doi/10.1061/JYCEAJ.0002369 doi: 10.1061/JYCEAJ.0002369
Hassan, M. A., Saletti, M., Johnson, J. P. L., Ferrer-Boix, C., Venditti, J. G., & Church, M. (2020, December). Experimental Insights Into the Threshold of Motion in Alluvial Channels: Sediment Supply and Streambed State. *Journal of Geophysical Research: Earth Surface*, *125*(12). Retrieved 2021-11-12, from https://onlinelibrary.wiley.com/doi/10.1029/2020JF005736 doi:

10.1029/2020JF005736

Helley, E. J. (1969). Field measurement of the initiation of large bed particle motion in Blue Creek near Klamath, California. *US Government Printing Office*.

Heyman, J., Bohorquez, P., & Ancey, C. (2016, October). Entrainment, motion, and deposition of coarse particles transported by water over a sloping mobile bed: TRANSPORT OF COARSE PARTICLES IN WATER. *Journal of Geophysical Research: Earth Surface*, *121*(10), 1931–1952. Retrieved 2023-07-29, from http://doi.wiley.com/10.1002/2015JF003672 doi: 10.1002/2015JF003672

Hodge, R. A., Sear, D. A., & Leyland, J. (2013, April). Spatial variations in surface sediment structure in riffle-pool sequences: a preliminary test of the Differential Sediment Entrainment Hypothesis (DSEH): Spatial Variations in Sediment Structure in Riffle-Pool Sequences. *Earth Surface Processes and Landforms*, *38*(5), 449–465. Retrieved 2021-11-12, from https://onlinelibrary.wiley.com/doi/10.1002/esp.3290 doi: 10.1002/esp.3290

Hurst, A. A., Anderson, R. S., & Crimaldi, J. P. (2021, May). Toward Entrainment Thresholds in Fluvial Plucking. *Journal of Geophysical Research: Earth Surface*, *126*(5). Retrieved 2021-11-12, from https://onlinelibrary.wiley.com/doi/10.1029/2020JF005944 doi: 10.1029/2020JF005944

James, C. S. (1990, January). Prediction of entrainment conditions for nonuniform, noncohesive sediments. *Journal of Hydraulic Research*, *28*(1), 25–41. Retrieved 2021-11-12, from https://www.tandfonline.com/doi/full/10.1080/00221689009499145 doi: 10.1080/00221689009499145

Johnston, C. E., Andrews, E. D., & Pitlick, J. (1998, August). In situ determination of particle friction angles of fluvial gravels. *Water Resources Research*, *34*(8), 2017–2030. Retrieved 2021-11-21, from http://doi.wiley.com/10.1029/98WR00312 doi: 10.1029/98WR00312

Kirchner, J. W., Dietrich, W. E., Iseya, F., & Ikeda, H. (1990, August). The variability of critical shear stress, friction angle, and grain protrusion in water-worked sediments. *Sedimentology*, *37*(4), 647–672. Retrieved 2022-04-06, from https://onlinelibrary.wiley.com/doi/10.1111/j.1365-3091.1990.tb00627.x doi: 10.1111/j.1365-3091.1990.tb00627.x

Komar, P. D., & Clemens, K. E. (1986). The Relationship Between a Grain's Settling Velocity and Threshold of Motion Under Unidirectional Currents. *SEPM Journal of Sedimentary Research*, *Vol. 56*. Retrieved 2021-11-12, from https://pubs.geoscienceworld.org/jsedres/article/56/2/258-266/113721 doi: 10.1306/212F88DC-2B24-11D7-8648000102C1865D

Lamb, M. P., Brun, F., & Fuller, B. M. (2017a, September). Direct measurements of lift and drag on shallowly submerged cobbles in steep streams: Implications for flow resistance and sediment transport. *Water Resources Research*, *53*(9), 7607–7629. Retrieved 2021-11-12, from https://onlinelibrary.wiley.com/doi/10.1002/2017WR020883 doi: 10.1002/2017WR020883

Lamb, M. P., Brun, F., & Fuller, B. M. (2017b, March). Hydrodynamics of steep streams with planar coarse-grained beds: Turbulence, flow resistance, and implications for sediment transport. *Water Resources Research*, *53*(3), 2240–2263. Retrieved 2021-11-12, from https://onlinelibrary.wiley.com/doi/10.1002/2016WR019579 doi: 10.1002/2016WR019579

Lamb, M. P., Dietrich, W. E., & Venditti, J. G. (2008, May). Is the critical Shields stress for incipient sediment motion dependent on channel-bed slope? *Journal of Geophysical Research*, *113*(F2), F02008. Retrieved 2021-11-12, from http://doi.wiley.com/10.1029/2007JF000831 doi: 10.1029/2007JF000831

Lee, H., & Balachandar, S. (2012, March). Critical shear stress for incipient motion of a particle on a rough bed: CRITICAL STRESS FOR INCIPIENT MO-

TION. *Journal of Geophysical Research: Earth Surface*, *117*(F1), n/a–n/a. Retrieved 2023-02-03, from http://doi.wiley.com/10.1029/2011JF002208 doi: 10.1029/2011JF002208

Lee, H., & Balachandar, S. (2017, January). Effects of wall roughness on drag and lift forces of a particle at finite Reynolds number. *International Journal of Multiphase Flow*, *88*, 116–132. Retrieved 2023-05-06, from https://linkinghub.elsevier.com/retrieve/pii/S0301932216300994 doi: 10.1016/j.ijmultiphaseflow.2016.09.006

Leliavsky, S. (1955). *An introduction to fluvial hydraulics.*

Li, X., Balachandar, S., Lee, H., & Bai, B. (2019, September). Fully resolved simulations of a stationary finite-sized particle in wall turbulence over a rough bed. *Physical Review Fluids*, *4*(9), 094302. Retrieved 2023-05-06, from https://link.aps.org/doi/10.1103/PhysRevFluids.4.094302 doi: 10.1103/PhysRevFluids.4.094302

López, R., & Barragán, J. (2008, June). Equivalent roughness of gravel-bed rivers. *Journal of Hydraulic Engineering*, *134*(6), 847–851. Retrieved 2022-04-13, from http://ascelibrary.org/doi/10.1061/%28ASCE%290733-9429%282008%29134%3A6%28847%29 doi: 10.1061/(ASCE)0733-9429(2008)134:6(847)

Maniatis, G., Hoey, T., Hodge, R., Rickenmann, D., & Badoux, A. (2020, December). Inertial drag and lift forces for coarse grains on rough alluvial beds measured using in-grain accelerometers. *Earth Surface Dynamics*, *8*(4), 1067–1099. Retrieved 2022-04-13, from https://esurf.copernicus.org/articles/8/1067/2020/ doi: 10.5194/esurf-8-1067-2020

Masteller, C. C., Finnegan, N. J., Turowski, J. M., Yager, E. M., & Rickenmann, D. (2019, March). History-dependent threshold for motion revealed by continuous bedload transport measurements in a steep mountain stream. *Geophysical Research Letters*, *46*(5), 2583–2591. Retrieved 2021-11-12, from https://onlinelibrary.wiley.com/doi/10.1029/2018GL081325 doi: 10.1029/2018GL081325

McKenna, F., Satish, A. B., Yi, S.-R., Zsarnoczay, A., Gardner, M., & Elhaddad, W. (2021, December). *NHERI-SimCenter/quoFEM: Version2.4.1.* Zenodo. Retrieved 2022-02-20, from https://zenodo.org/record/5800081 doi: 10.5281/ZENODO.5800081

Metropolis, N., & Ulam, S. (1949). The Monte Carlo Method. *Journal of the American statistical association*, *44*(247), 335–341.

Meyer-Peter, & Müller. (1948). Formulas for bed-load transport. *IAHSR 2nd meeting, Stockholm, appendix 2.*

Mueller, E. R., Pitlick, J., & Nelson, J. M. (2005, April). Variation in the reference Shields stress for bed load transport in gravel-bed streams and rivers. *Water Resources Research*, *41*(4). Retrieved 2022-02-20, from http://doi.wiley.com/10.1029/2004WR003692 doi: 10.1029/2004WR003692

Paintal, A. S. (1971, January). Concept of critical shear stress in loose boundary open channels. *Journal of Hydraulic Research*, *9*(1), 91–113. Retrieved 2021-11-12, from https://www.tandfonline.com/doi/full/10.1080/00221687109500339 doi: 10.1080/00221687109500339

Parker, G. (1978, November). Self-formed straight rivers with equilibrium banks and mobile bed. Part 2. The gravel river. *Journal of Fluid Mechanics*, *89*(1), 127–146. Retrieved 2023-03-28, from https://www.cambridge.org/core/product/identifier/S0022112078002505/type/journal_article doi: 10.1017/S0022112078002505

Parker, G. (1991, February). Selective Sorting and Abrasion of River Gravel. II: Applications. *Journal of Hydraulic Engineering*, *117*(2), 150–171. Retrieved 2023-02-20, from https://ascelibrary.org/doi/10.1061/%28ASCE%290733-9429%281991%29117%3A2%28150%29 doi: 10.1061/(ASCE)0733-9429(1991)117:2(150)

Perron, J. T., Lamb, M. P., Koven, C. D., Fung, I. Y., Yager, E., & Ádámkovics, M. (2006, November). Valley formation and methane precipitation rates on Titan. *Journal of Geophysical Research*, *111*(E11), E11001. Retrieved 2021-11-12, from `http://doi.wiley.com/10.1029/2005JE002602` doi: 10.1029/2005JE002602

Pfeiffer, A. M., Finnegan, N. J., & Willenbring, J. K. (2017, March). Sediment supply controls equilibrium channel geometry in gravel rivers. *Proceedings of the National Academy of Sciences*, *114*(13), 3346–3351. Retrieved 2023-02-20, from `https://pnas.org/doi/full/10.1073/pnas.1612907114` doi: 10.1073/pnas.1612907114

Phillips, C. B., Masteller, C. C., Slater, L. J., Dunne, K. B. J., Francalanci, S., Lanzoni, S., ... Jerolmack, D. J. (2022, May). Threshold constraints on the size, shape and stability of alluvial rivers. *Nature Reviews Earth & Environment*, *3*(6), 406–419. Retrieved 2023-02-20, from `https://www.nature.com/articles/s43017-022-00282-z` doi: 10.1038/s43017-022-00282-z

Pierce, J. K., Hassan, M. A., & Ferreira, R. M. L. (2022, August). Probabilistic description of bedload fluxes from the aggregate dynamics of individual grains. *Earth Surface Dynamics*, *10*(4), 817–832. Retrieved 2023-07-29, from `https://esurf.copernicus.org/articles/10/817/2022/` doi: 10.5194/esurf-10-817-2022

Prancevic, J. P., & Lamb, M. P. (2015, February). Particle friction angles in steep mountain channels: Friction angles in mountain channels. *Journal of Geophysical Research: Earth Surface*, *120*(2), 242–259. Retrieved 2021-11-12, from `http://doi.wiley.com/10.1002/2014JF003286` doi: 10.1002/2014JF003286

Prancevic, J. P., Lamb, M. P., & Fuller, B. M. (2014, March). Incipient sediment motion across the river to debris-flow transition. *Geology*, *42*(3), 191–194. Retrieved 2022-02-20, from `http://pubs.geoscienceworld.org/geology/article/42/3/191/131486/Incipient-sediment-motion-across-the-river-to` doi: 10.1130/G34927.1

Pähtz, T., Clark, A. H., Valyrakis, M., & Durán, O. (2020, March). The Physics of Sediment Transport Initiation, Cessation, and Entrainment Across Aeolian and Fluvial Environments. *Reviews of Geophysics*, *58*(1). Retrieved 2023-01-31, from `https://onlinelibrary.wiley.com/doi/abs/10.1029/2019RG000679` doi: 10.1029/2019RG000679

Recking, A. (2009, April). Theoretical development on the effects of changing flow hydraulics on incipient bed load motion: INCIPIENT MOTION CONDITIONS. *Water Resources Research*, *45*(4). Retrieved 2023-03-03, from `http://doi.wiley.com/10.1029/2008WR006826` doi: 10.1029/2008WR006826

Riebe, C. S., Sklar, L. S., Overstreet, B. T., & Wooster, J. K. (2014, February). Optimal reproduction in salmon spawning substrates linked to grain size and fish length: OPTIMAL REPRODUCTION IN SALMON SPAWNING SUBSTRATES. *Water Resources Research*, *50*(2), 898–918. Retrieved 2023-02-20, from `http://doi.wiley.com/10.1002/2013WR014231` doi: 10.1002/2013WR014231

Scheingross, J. S., Winchell, E. W., Lamb, M. P., & Dietrich, W. E. (2013, June). Influence of bed patchiness, slope, grain hiding, and form drag on gravel mobilization in very steep streams. *Journal of Geophysical Research: Earth Surface*, *118*(2), 982–1001. Retrieved 2022-02-20, from `http://doi.wiley.com/10.1002/jgrf.20067` doi: 10.1002/jgrf.20067

Schmeeckle, M. W., Nelson, J. M., & Shreve, R. L. (2007, April). Forces on stationary particles in near-bed turbulent flows. *Journal of Geophysical Research*, *112*(F2), F02003. Retrieved 2021-11-12, from `http://doi.wiley.com/10.1029/2006JF000536` doi: 10.1029/2006JF000536

Seminara, G., Solari, L., & Parker, G. (2002, November). Bed load at low Shields stress on arbitrarily sloping beds: Failure of the Bagnold hypothesis: FAILURE OF THE BAGNOLD HYPOTHESIS. *Water Resources Research*, *38*(11), 31–1–31–16. Retrieved 2023-07-29, from http://doi.wiley.com/10.1029/2001WR000681 doi: 10.1029/2001WR000681

Shields, A. (1936). Application of similarity principles and turbulence research to bed-load movement.

Shvidchenko, A. B., Pender, G., & Hoey, T. B. (2001, August). Critical shear stress for incipient motion of sand/gravel streambeds. *Water Resources Research*, *37*(8), 2273–2283. Retrieved 2022-02-20, from http://doi.wiley.com/10.1029/2000WR000036 doi: 10.1029/2000WR000036

Smart, G., & Habersack, H. (2007, September). Pressure fluctuations and gravel entrainment in rivers. *Journal of Hydraulic Research*, *45*(5), 661–673. Retrieved 2023-03-08, from https://www.tandfonline.com/doi/full/10.1080/00221686.2007.9521802 doi: 10.1080/00221686.2007.9521802

Sobol, I. (2001, February). Global sensitivity indices for nonlinear mathematical models and their Monte Carlo estimates. *Mathematics and Computers in Simulation*, *55*(1-3), 271–280. Retrieved 2022-02-20, from https://linkinghub.elsevier.com/retrieve/pii/S0378475400002706 doi: 10.1016/S0378-4754(00)00270-6

Strand, R. (1973). *Sedimentation, in U.S. Bureau of Reclamation, Design of small dams.* Washington, D. C., U.S. Government Printing Office.

Turowski, J. M. (2010, August). Probability distributions of bed load transport rates: A new derivation and comparison with field data: PROBABILITY DISTRIBUTIONS OF BEDLOAD TRANSPORT. *Water Resources Research*, *46*(8). Retrieved 2023-07-29, from http://doi.wiley.com/10.1029/2009WR008488 doi: 10.1029/2009WR008488

Vollmer, S., & Kleinhans, M. G. (2007, May). Predicting incipient motion, including the effect of turbulent pressure fluctuations in the bed: PREDICTING INCIPIENT MOTION. *Water Resources Research*, *43*(5). Retrieved 2023-03-03, from http://doi.wiley.com/10.1029/2006WR004919 doi: 10.1029/2006WR004919

Whitaker, A. C., & Potts, D. F. (2007, July). Analysis of flow competence in an alluvial gravel bed stream, Dupuyer Creek, Montana. *Water Resources Research*, *43*(7). Retrieved 2022-02-20, from http://doi.wiley.com/10.1029/2006WR005289 doi: 10.1029/2006WR005289

Wiberg, P. L., & Smith, J. D. (1987, August). Calculations of the critical shear stress for motion of uniform and heterogeneous sediments. *Water Resources Research*, *23*(8), 1471–1480. Retrieved 2021-11-12, from http://doi.wiley.com/10.1029/WR023i008p01471 doi: 10.1029/WR023i008p01471

Wickert, A. D., & Schildgen, T. F. (2019, January). Long-profile evolution of transport-limited gravel-bed rivers. *Earth Surface Dynamics*, *7*(1), 17–43. Retrieved 2023-02-23, from https://esurf.copernicus.org/articles/7/17/2019/ doi: 10.5194/esurf-7-17-2019

Williams, R. M. E., Grotzinger, J. P., Dietrich, W. E., ..., & Moores, J. E. (2013, May). Martian Fluvial Conglomerates at Gale Crater. *Science*, *340*(6136), 1068–1072. Retrieved from https://www.science.org/doi/10.1126/science.1237317 doi: 10.1126/science.1237317

Wohl, E., Bledsoe, B. P., Jacobson, R. B., Poff, N. L., Rathburn, S. L., Walters, D. M., & Wilcox, A. C. (2015, April). The Natural Sediment Regime in Rivers: Broadening the Foundation for Ecosystem Management. *BioScience*, *65*(4), 358–371. Retrieved 2023-02-20, from http://academic.oup.com/bioscience/article/65/4/358/254680/The-Natural-Sediment-Regime-in-Rivers-Broadening doi: 10.1093/biosci/biv002

Wong, M., & Parker, G. (2006, November). Reanalysis and Correction of Bed-Load

Relation of Meyer-Peter and Müller Using Their Own Database. *Journal of Hydraulic Engineering*, *132*(11), 1159–1168. Retrieved 2023-05-14, from https://ascelibrary.org/doi/10.1061/%28ASCE%290733-9429%282006%29132%3A11%281159%29 doi: 10.1061/(ASCE)0733-9429(2006)132:11(1159)

Wu, F.-C., & Shih, W.-R. (2012, September). Entrainment of sediment particles by retrograde vortices: Test of hypothesis using near-particle observations. *Journal of Geophysical Research: Earth Surface*, *117*(F3), n/a–n/a. Retrieved 2021-11-21, from http://doi.wiley.com/10.1029/2011JF002242 doi: 10.1029/2011JF002242

Yager, E. M., Kirchner, J. W., & Dietrich, W. E. (2007, July). Calculating bed load transport in steep boulder bed channels: SEDIMENT TRANSPORT IN STEEP CHANNELS. *Water Resources Research*, *43*(7). Retrieved 2023-02-20, from http://doi.wiley.com/10.1029/2006WR005432 doi: 10.1029/2006WR005432

Yager, E. M., Schmeeckle, M. W., & Badoux, A. (2018, December). Resistance is not futile: Grain resistance controls on observed critical Shields stress variations. *Journal of Geophysical Research: Earth Surface*, *123*(12), 3308–3322. Retrieved 2021-11-12, from https://onlinelibrary.wiley.com/doi/10.1029/2018JF004817 doi: 10.1029/2018JF004817

Yager, E. M., Venditti, J. G., Smith, H. J., & Schmeeckle, M. W. (2018, December). The trouble with shear stress. *Geomorphology*, *323*, 41–50. Retrieved 2023-02-03, from https://linkinghub.elsevier.com/retrieve/pii/S0169555X18303659 doi: 10.1016/j.geomorph.2018.09.008